Available online at www.sciencedirect.com

ScienceDirect

Scripta Materialia 93 (2014) 48–51

Scripta MATERIALIA

www.elsevier.com/locate/scriptamat

# X-ray microbeam measurements of long-range internal stresses in commercial-purity aluminum processed by multiple passes of equal-channel angular pressing

Thien Q. Phan,[a,*] I-Fang Lee,[a] Lyle E. Levine,[b] Jonathan Z. Tischler,[c] Yi Huang,[d] Alan G. Fox,[e] Terence G. Langdon[a,d] and Michael E. Kassner[a]

[a] *Departments of Aerospace & Mechanical Engineering and Materials Science, University of Southern California, Los Angeles, CA 90089-1453, USA*

[b] *Material Measurement Laboratory, National Institute of Standards and Technology, Gaithersburg, MD 20899-8553, USA*

[c] *Advanced Photon Source, Argonne National Laboratory, Argonne, IL 60439-4800, USA*

[d] *Materials Research Group, Faculty of Engineering and the Environment, University of Southampton, Southampton SO17 1BJ, UK*

[e] *Mechanical Engineering Department, Asian University, 89 Moo 12, Highway 331, Banglamung, Chon Buri 20260, Thailand*

Received 30 April 2014; revised 14 August 2014; accepted 4 September 2014
Available online 18 September 2014

X-ray microbeam diffraction was used to measure long-range internal stresses (LRISs) in the grain/subgrain interiors of commercial-purity aluminum processed by equal-channel angular pressing for up to eight passes. The LRIS values at +4.9° off the axial (pressing) direction show only a slight increase with increasing numbers of passes. The normalized stress remains approximately constant at ~0.10 of the flow stress.


*Keywords:* X-ray diffraction; Aluminum; Equal-channel angular pressing; Long-range internal stresses; Severe plastic deformation

Severe plastic deformation (SPD) has been a popular method for producing materials with refined grain sizes [1–3]. This grain refinement leads to improved mechanical properties including hardness, yield strength and fracture toughness. One attractive SPD technique is equal-channel angular pressing (ECAP) [4–6], which produces relatively homogeneous refined grain-sizes in bulk material. Grain refinement occurs primarily via the formation of geometrically necessary boundaries [7]. These boundaries may be nonequilibrium and have many emanating or extrinsic dislocations [8,9]. Thus, these boundaries may also be sources for the relatively high long-range internal stresses (LRISs) observed by Alhajeri et al. [10] for aluminum 1050. Recent work by the authors examined the LRISs in the subgrain/grain interiors of the Alhajeri et al. aluminum specimens using X-ray microbeam diffraction at a synchrotron [11]. The results of the LRIS evaluation of the subgrain/grain walls and their interiors were consistent with the composite model [24], at least for one pass of ECAP. The original composite model [24] describes "hard" high dislocation density regions (e.g. cell walls, etc.) and "soft" regions of low dislocation density (e.g. cell interiors). This creates regions of high and low stress as the "composite" is strained compatibly. In practice, the stresses are also consistent with the summation of the stress fields of the dislocations. The model is reviewed in detail in Ref. [19]. In this report, a microbeam diffraction evaluation of LRISs using ECAP AA1050 processed for multiple passes is now presented as a continuation of the earlier work [11]. Commercial-purity aluminum was utilized both for relevance to commercial applications and because it is less subject to dynamic recrystallization [12].

The internal elastic strains of the low dislocation density regions within the grains/subgrains of ECAP AA1050 along the pressing direction for 1, 2, 4 and 8 passes were measured using microbeam X-ray diffraction at beam line 34ID-E of the Advanced Photon Source (APS) at Argonne National Laboratory. Only a single reflection could be measured from each grain, providing information on the elastic strain in just a single direction with respect to the sample geometry. Obtaining complete strain tensors may be possible by measuring multiple reflections but that is beyond the scope of the current study.

The ECAP AA1050 composition, machining and other experimental procedures are identical to those used in our

* Corresponding author; e-mail: thienqph@usc.edu

http://dx.doi.org/10.1016/j.scriptamat.2014.09.001
1359-6462/

previous study [11]. Ideally, the ECAP die imposes approximately +0.88 principal plastic strain for each pass along the +22.5° direction, −0.88 plastic strain along the −67.5° direction off the pressing direction and about zero plastic strain along the pressing direction [13] after a single pass and in the plane deformed by the extrusion axis as illustrated in Figure 1. The ECAP die imposes roughly +0.19 plastic strain, or about 21% of the maximum plastic strain for our measurement direction (about +5° off the pressing axis) after a single ECAP pass. The ECAP AA1050 samples were processed via route $B_C$, with samples rotated by 90° between each pass [14–16]. Samples subjected to 1, 2, 4 and 8 passes were examined.

The powder diffraction measurement procedures were identical to those described earlier [11]. Lattice parameters were measured using X-ray powder diffraction for the as-received (pre-ECAP) condition and after 1, 2, 4 and 8 passes (P). The lattice parameter for the as-received AA1050 was 4.05000(10) Å, for 1P: 4.05020(10) Å, for 2P: 4.05010(10) Å, for 4P: 4.05010(10) Å and for 8P: 4.05010(10) Å. These lattice parameters show little variation between the number of passes with all values lying within one standard deviation of 4.05010 Å, which suggests that these samples exhibit negligible residual stresses on length scales that are large compared to dislocation microstructures. The lattice parameter obtained from the as-received AA1050 sample was used as the baseline $a_o$. We note that this lattice parameter is slightly different from the pure Al lattice parameter of 4.04950(15) Å [17] that is generally used in other AA1050 LRIS studies. The difference in lattice parameter from pure Al and 1050 Al multiplied by Young's modulus translates to (an equivalent strain) error of $+10^{-4}$, which is significant. The radii of Al, Si and Fe are 0.118, 0.111 and 0.156 nm, respectively. The composition of AA1050 is 0.25% Si, 0.4% Fe. Using a simple weighted average and hard sphere model, at least a $10^{-4}$ increase in $a_0$ is expected. As mentioned above, we find that using a (powder) diffraction measurement on the 11-BM beamline at the APS, the average lattice parameter is constant (over a beam diameter of 3 mm) for all specimen passes. Thus, there is no evidence of macroscopic residual stresses in ECAP AA1050. Macroscopic residual stresses, however, were observed in separate work on ECAP AA6005.

X-ray microbeam diffraction measurements on beamline 34-ID-E at the APS were performed identically to those reported previously [11], with a microbeam cross-section of approximately 500 nm × 500 nm. The {5 3 1} reflections were used to obtain lattice spacings for each of the samples. Lattice spacings measured by the X-ray microbeams were obtained from relatively low dislocation density areas within the grain/subgrain interiors that produce sharp diffraction spots on the detector. The measured lattice spacings were then compared to powder-diffraction-based lattice parameters to calculate elastic strains within these regions. Lattice parameter measurements in high dislocation density regions (cell walls) were made on strained (0.30 strain) Cu in an earlier work by the authors [23]. There, the walls are diffuse and less well-defined, and X-ray peak positions could be reasonably assessed. However, in ECAP, the cell walls/grain boundaries had much higher dislocation densities that precluded identifying well-defined X-ray peaks and corresponding lattice parameters. Within the cell interiors there were higher dislocation density regions with more X-ray scattering, and lower dislocation density regions with less X-ray scattering. The lower dislocation density regions were associated with better-defined peaks and thus easier strain or lattice parameter measurements. We chose to measure the better-defined peaks of the cell interiors.

After 1, 2, 4 and 8 ECAP passes, the microstructure of a similar Al specimen exhibits grains with boundaries of mixed high and low misorientation angles [7] as is typical for SPD [18]. After 1 pass, about 15–20% of the boundaries are high-angle grain boundaries (HAGBs) having misorientations >15° according to transmission electron microscopy (TEM) (rather than electron backscatter diffraction that may not detect all low-angle boundaries). Similarly, after 2 passes the HAGB fraction is ~25%, after 4 passes it is ~37% and after 8 passes it is ~70% [7]. According to TEM analysis, the average grain/subgrain size formed by high- and low-angle grain boundaries is about 1 μm for 2 passes, 900 nm for 4 passes, and 680 nm for 8 passes [10].

In earlier work on deformed Cu [23], it was possible to directly measure the elastic strains within the high dislocation density cell walls. Here, the sharp grain boundaries of ECAP AA1050 provided too little scattered intensity distributed over too large an area of the detector to allow direct strain measurements from these boundaries. Within

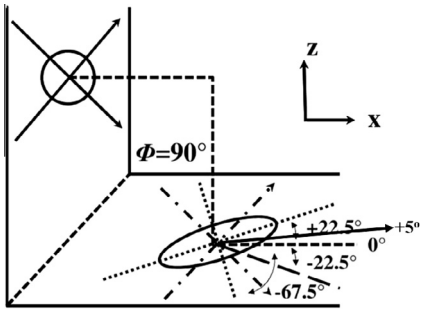


**Figure 1.** A circle is deformed into an ellipse after ECAP processing. The long axis (+22.5°) of the ellipse indicates the maximum tensile plastic strain. Strain along the pressing axis (0°) is theoretically zero [13]. Strain measurements are made along the +5° direction.

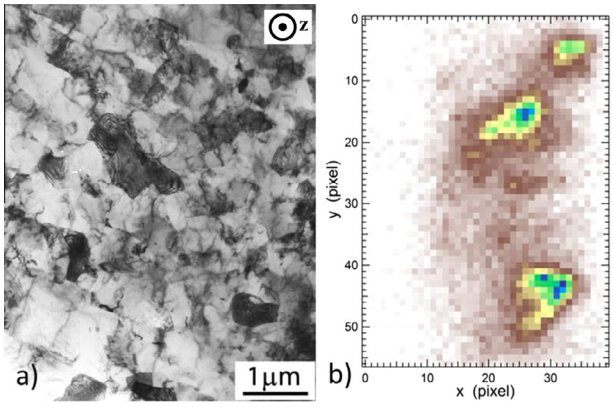


**Figure 2.** (a) TEM image of ECAP AA1050 after 2 passes. (b) False-color image of the energy-integrated diffracted intensity from an individual grain/subgrain in a 2-pass sample. The peaks are from low-dislocation-density regions and the smeared intensity is from walls or cell interiors with a relatively high dislocation density, (b) is taken from earlier work on the same alloy [11].

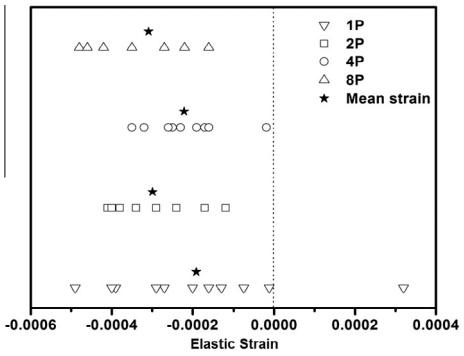


**Figure 3.** The distribution of elastic strains within low-dislocation-density regions of AA1050 subgrain/grain interiors after 1, 2, 4 and 8 ECAP passes. The strains are characterized at the center of the sample, at approximately +5° off the pressing axis. Each star represents the average value for each set of data from a given number of ECAP passes. Compressive stresses are expected in cell interiors to balance the strain/stress associated with an overall positive (tensile) strain.

the ECAP grains, dislocations are distributed heterogeneously. Figure 2a shows a representative TEM image of ECAP AA1050 after two passes. The microbeam X-ray diffraction data reflects the heterogeneity of the dislocation distribution within the grains/subgrains as shown in Figure 2b (diffraction image is taken from earlier work on the same alloy [11]). Here, the peaks originate from low dislocation areas and the smeared intensity is from high dislocation areas both from boundaries and high dislocation density regions within the grain/subgrain. The different positions of the peaks in the image reflect the local crystallographic misorientations of the low dislocation density regions (within a single grain/subgrain). The apparent misorientation between the upper and lower spots in Figure 2b is 0.9°. All lattice parameter measurements were conducted on well-defined peaks such as those shown in Figure 2b.

Figure 3 illustrates all of the elastic strain measurements obtained from the centers of the AA1050 ECAP samples nearly along the pressing axis after 1, 2, 4 and 8 passes. Due to the geometry of the diffracted spots, sample and detector, strains were measured slightly off the pressing direction. The {5 3 1} lattice spacings were measured within ~5.0° of the pressing direction. These lattice spacings were converted to strains using the unstrained lattice parameter.

Figure 3 shows that most of the measured elastic strains are negative except for one value from the 1-pass sample. Under ideal conditions, the expected strain along the +5° direction is +0.19 after each pass, so the composite model for internal stresses predicts a negative (compressive) LRIS in the grain/subgrain interiors [19] in this orientation as was observed for all ECAP samples. Thus, the LRISs very near the boundaries are expected to be positive. Although the orientation of the strain tensor very near the boundaries was not determined by Alhajeri et al. [10], they in fact observed a positive maximum principal strain that corresponded to $\sim 0.75\sigma_a$ (for 2 passes). Therefore, the corresponding stress in the grain interiors is expected to be negative, as was observed in the +22.5° (after one pass [11]) and +5° directions in the current work for 1–8 passes (see Fig. 1).

Table 1 shows the mean elastic strain of the grain interiors of the ECAP samples, together with the standard deviation and the uncertainty, or standard error, of the mean value (standard deviation divided by the square root of the number of datum points used to calculate the mean). While all of the mean elastic strains are negative, the width of the strain distribution for the 1-pass specimen is significantly (~2 times) larger than for the multiple-pass specimens. The standard deviation for the 1-pass specimen is $2.2 \times 10^{-4}$ compared to $\sim 1 \times 10^{-4}$ for the samples that have undergone multiple ECAP passes. There is no significant difference between the spread of the strain distribution for the 2-, 4- and 8-pass samples.

The mean elastic strain values of the low dislocation density regions within the grain/subgrains of all samples vary from $-1.9 \times 10^{-4}$ to $-3.1 \times 10^{-4}$ from the low to high number of passes, with the uncertainty ranging from $3.0 \times 10^{-5}$ to $6.7 \times 10^{-5}$. The LRIS increases slightly with the number of passes while the normalized LRIS remains approximately unchanged. The measured mean elastic axial strain of the cell interiors for the 1-, 2-, 4- and 8-pass samples are $-1.9 \times 10^{-4}$, $-3.0 \times 10^{-4}$, $-2.2 \times 10^{-4}$ and $-3.1 \times 10^{-4}$, respectively. These values convert to about −13.6, −21.2, −15.7 and −21.9 MPa LRISs for 1, 2, 4 and 8 passes, respectively (Young's modulus along the <5 3 1> direction ~71 GPa [20]). This equates to 0.09, 0.14, 0.08 and $0.10\sigma_a$ for 1, 2, 4 and 8 passes (flow stress $\sigma_a \approx 148$, 150, 180 and 200 MPa for 1, 2, 4 and 8 passes, respectively [21]). Table 1 shows no clear trend between the number of passes and the LRISs as a fraction of the flow stress for different ECAP passes. The variations in magnitude of the normalized LRISs are considered insignificant.

Our results indicate that compressive internal elastic strains along the pressing direction are present within low dislocation density regions for all ECAP passes. Again, multiple-pass ECAP samples were pressed using route $B_C$, which dictates that specimens are rotated by 90° between each pass. This means that the cumulative maximum plastic strain direction would no longer correspond to the +22.5° direction and the minimum plastic strain direction would no longer be along the −67.5° direction for multiple-pass specimens. It is unclear in multipass specimens how the deformation history affects the LRIS after the final pass. Thus, the elastic strain values from multiple ECAP pass samples are not easily compared to the 1-pass sample where the maximum strain is near the +22.5° direction. Again, the situation is additionally complicated by the fact that the ECAP process is non-ideal with respect to the maximum

**Table 1.** The mean values, deviation and uncertainty of mean values for the measured strains of low dislocation regions of AA1050 aluminum after 1, 2, 4 and 8 ECAP passes.

| No. of passes | 1 (Lee et al. [11]) | 2 | 4 | 8 |
|---|---|---|---|---|
| Mean elastic strain | $-1.9 \times 10^{-4}$ | $-2.99 \times 10^{-4}$ | $-2.21 \times 10^{-4}$ | $-3.09 \times 10^{-4}$ |
| Standard deviation | $2.24 \times 10^{-4}$ | $1.04 \times 10^{-4}$ | $9.34 \times 10^{-5}$ | $1.20 \times 10^{-4}$ |
| Uncertainty of mean value | $6.74 \times 10^{-5}$ | $3.28 \times 10^{-5}$ | $2.95 \times 10^{-5}$ | $3.79 \times 10^{-5}$ |
| Long-range internal stress (LRIS) (MPa) | −13.6 | −21.2 | −15.7 | −21.9 |
| Normalized stress ($\sigma_{LRIS}/\sigma_a$) | 0.09 | 0.14 | 0.08 | 0.10 |

plastic strain axes as the die is associated with friction, adiabatic heating, non-ideal die geometry, etc. With multiple passes using the $B_c$ route, the maximum principal strain direction probably rotates about the pressing axis.

In conclusion, X-ray microbeam diffraction measurements of a commercial-purity AA1050 alloy processed by multiple-pass ECAP consistently reveals negative elastic strains within +4.9° of the pressing axis direction within grain/subgrain interiors. The average elastic strains for 1, 2, 4 and 8 passes were $-1.9 \times 10^{-4}$, $-3.0 \times 10^{-4}$, $-2.2 \times 10^{-4}$ and $-3.1 \times 10^{-4}$ which equate to approximately $0.09\sigma_a$, $0.14\sigma_a$, $0.08\sigma_a$ and $0.10\sigma_a$, respectively. There is a slight trend of increasing elastic strain with the number of ECAP passes along the +4.9° direction. The normalized LRIS is approximately independent of strain. This work, together with the earlier report by Lee et al. [11] and Alhajeri et al. [10], who used convergent beam electron diffraction to assess the LRISs near grain/subgrain boundaries, suggest the existence of LRISs in ECAP AA1050 and the results appear consistent with the composite model. These results complement the earlier work by the authors in which only one pass was examined. The present work suggests that the LRIS only modestly increases with plastic strain and the normalized LRIS is essentially constant. The results also show that, because of the relatively small volume fraction of boundaries, the LRIS in the dislocation walls is relatively high ($0.75\sigma_a$) and may exceed those in other deformation-induced boundaries where the LRIS in the dislocation walls was found to be relatively low [19,22,23]. The volume and LRIS of the interior compensates the volume and LRIS of the walls for a zero net stress in the unloaded material. Due to the complexity of loading during ECAP (the polycrystalline nature of the specimen, friction effects, etc.), it is ideal to measure strains along different directions in order to approach a full tensor. However, we do not currently have the ability to measure full strain within a given grain. Future efforts are being made in order to measure strains along independent directions and thus determine the full strain tensor within a particular grain.

Research at the University of Southern California was supported the National Science Foundation through DMR-1401194, the XOR/UNI facilities on 11-BM and 34ID at the APS are supported by the DOE Office of Science under Contract No. DE-AC02-06CH11357, and research at the University of Southampton was supported by the European Research Council under ERC Grant Agreement No. 267464-SPDMETALS.

[1] M.A. Meyers, A. Mishra, D.J. Benson, Prog. Mater. Sci. 51 (2006) 427–556.
[2] R.Z. Valiev, Y. Estrin, Z. Horita, T.G. Langdon, M.J. Zehetbauer, Y.T. Zhu, JOM 58 (4) (2006) 33–39.
[3] Y. Zhu, R.Z. Valiev, T.G. Langdon, N. Tsuji, K. Lu, MRS Bull. 35 (2010) 977–981.
[4] Y. Iwahashi, M. Furukawa, Z. Horita, M. Nemoto, T.G. Langdon, Metall. Mater. Trans. A 29A (1998) 2245–2252.
[5] G.J. Raab, R.Z. Valiev, T.C. Lowe, Y.T. Zhu, Mater. Sci. Eng. A 382 (2004) 30–34.
[6] R.Z. Valiev, T.G. Langdon, Prog. Mater. Sci. 51 (2006) 881–981.
[7] M. Cabibbo, E. Evangelista, M.E. Kassner, M.A. Meyers, W. Blum, Metall. Mater. Trans. A 39 (2008) 181–189.
[8] Z. Horita, D.J. Smith, M. Furukawa, M. Nemoto, R.Z. Valiev, T.G. Langdon, J. Mater. Res. 11 (1996) 1880–1890.
[9] H.Z. Ding, H. Mughrabi, H.W. Hoppel, Fatigue Fract. Eng. Mater. Struct. 25 (2002) 975–984.
[10] S.N. Alhajeri, A.G. Fox, T.G. Langdon, Acta Mater. 59 (2011) 7388–7395.
[11] I.F. Lee, T.Q. Phan, L.E. Levine, J.Z. Tischler, P.T. Geantil, Y. Huang, T.G. Langdon, M.E. Kassner, Acta Mater. 61 (2013) 7741–7748.
[12] M.E. Kassner, J. Pollard, E. Evangelista, E. Cerri, Acta Mater. 42 (1994) 3223–3230.
[13] K. Xia, J. Wang, Metall. Mater. Trans. A 32 (2001) 2639–2647.
[14] M. Furukawa, Y. Iwahashi, Z. Horita, M. Nemoto, T.G. Langdon, Mater. Sci. Eng. A 257 (1998) 328–332.
[15] M. Kawasaki, Z. Horita, T.G. Langdon, Mater. Sci. Eng. A 524 (2009) 143–150.
[16] S.N. Alhajeri, N. Gao, T.G. Langdon, Mater. Sci. Eng. A 528 (2011) 3833–3840.
[17] W. Witt, Zeitschrift fuer Naturforschung, Teil A. Physikalische Chemie. Kosmophysik 22 (1967) 92–95.
[18] M.E. Kassner, Metall. Mater. Trans. A 20A (1989) 2001–2010.
[19] M.E. Kassner, P. Geantil, L.E. Levine, Int. J. Plasticity 45 (2013) 44–60.
[20] C.L. Davis, M. Strangwood, M. Potter, S. Dixon, P.F. Morris, Metall. Mater. Trans. A 39A (2008) 679–687.
[21] C.Y. Yu, P.L. Sun, P.W. Kao, C.P. Chang, Scr. Mater. 52 (2005) 359–363.
[22] M.E. Kassner, M.T. Perez-Prado, K.S. Vecchio, M.A. Wall, Acta Mater. 48 (2000) 4247–4734.
[23] L.E. Levine, P. Geantil, B.C. Larson, T.Z. Tischler, M.E. Kassner, W. Liu, M.R. Stoudt, F. Tavazzd, Acta Mater. 54 (2011) 5083–5091.
[24] H. Mughrabi, Acta Mater. 31 (1983) 1367–1379.